

# Pauli web of the $|Y\rangle$ state surface code injection

Kwok Ho Wan<sup>1,2</sup> and Zhenghao Zhong<sup>2,1</sup>

<sup>1</sup>Blackett Laboratory, Imperial College London, South Kensington, London SW7 2AZ, UK

<sup>2</sup>Mathematical Institute, University of Oxford, Andrew Wiles Building, Woodstock Road, Oxford OX2 6GG, UK  
March 21, 2025

We employ ZX-calculus and Pauli web to understand the  $|Y\rangle$  state injection on the rotated surface code.

## 1 Introduction

Magic states ( $|T\rangle \propto |0\rangle + \exp(i\pi/4)|1\rangle$ ) are resource states in fault-tolerant quantum computation [1, 2]. One main challenge in practical fault-tolerant quantum computation is to encode such state from a bare physical  $|T\rangle$  state to an encoded logical  $|\bar{T}\rangle$  state on the surface code [3, 4]. We explore the state injection procedures [5, 6] with ZX-calculus [7, 8], specifically using Pauli webs [9, 10]. This allows a diagrammatic way to understand these procedures. The ZX-diagrams and Pauli webs provide hints at the importance of the upper and lower triangular located initial qubits in these protocols [5, 6].

We study a simpler injected state, injecting the  $|Y\rangle \propto |0\rangle + \exp(i\pi/2)|1\rangle$  state in place of the  $|T\rangle$  state. The choice for injecting the  $|Y\rangle$  state is motivated by its Clifford nature [2], this allows a full end-to-end analysis using Pauli web. In addition, we follow the Pauli web colouring scheme of [10] (opposite Pauli web colour highlighting compared to [9]). We assume knowledge of ZX-calculus, Pauli web and error correction with the surface code throughout this text. Please refer to [4, 9, 10] for detailed discussions.

The main aim of this brief communication is to show that the Pauli web produced in the Li/Lao-Criger [5, 6]  $|Y\rangle$  state injection schemes does indeed recover the logical  $Y$  correlator Pauli web (see detailed discussion in [9]) of the rotated surface code, as expected.

---

Kwok Ho Wan: [kwok.wan14@imperial.ac.uk](mailto:kwok.wan14@imperial.ac.uk)

## 2 Li/Lao-Criger state injection schemes

Li constructed a scheme to inject states onto the regular un-rotated surface code with high fidelity [5]. This was further generalised to the rotated surface code by Lao and Criger [6]. We will work exclusively with the Lao-Criger scheme with an injected  $|Y\rangle$  state physical qubit on the corner of a rotated surface code. In figure 1, we write the initial state proposed by [6] in the ZX-calculus notation. Time goes from bottom to top in all ZX-diagram. For illustration purposes, a distance  $d = 5$  surface code will be used throughout this text.

### 2.1 Initialisation

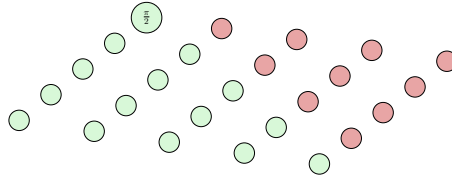


Figure 1: The initial state to the injection schemes [5, 6] written as a ZX-diagram. Upper left corner qubit initialised in the  $|Y\rangle \propto |0\rangle + i|1\rangle$  state ( $\frac{\pi}{2}$  phase green Z-spider). The lower triangular and diagonally located qubits in the  $|+\rangle$  state and the upper triangular located qubits in the  $|0\rangle$  state.

For a distance  $d$  surface code, a square grid of  $d \times d$  physical (data) qubits need to be initialised. A bare physical  $|Y\rangle$  state is initialised in the top left corner. The rest of the  $d^2 - 1$  data qubits will be initialised in  $|+\rangle$  state if they are located in the the lower triangular and main diagonal, and in the  $|0\rangle$  state if they sit along the upper triangular locations.

### 2.2 Encoder circuit and logical correlators

After the state initialisation, the surface code encoding circuit is applied to the state. This encoding circuit following the notation of [9] is shown in figure 2. This constitutes a full round of parity measurement. Measuring all the  $XXXX/XX$  plaquettes parity measurements in the first layer followed by the  $ZZZZ/ZZ$  equivalents in the second layer.

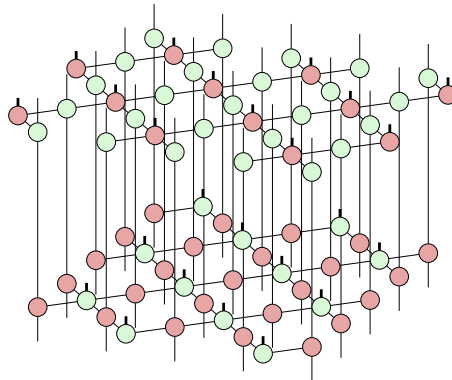


Figure 2: An error-free (distance  $d = 5$ ) rotated surface code encoder circuit. This consists of X-type followed by Z-type plaquette parity measurements (for detailed discussion, see [4, 9]).

The surface code encoder have logical  $Z$  or  $X$  correlators [9] that connects the  $Z$  or  $X$  logical operators from the input to output of the ZX-diagram (bottom to top). In figure 3,

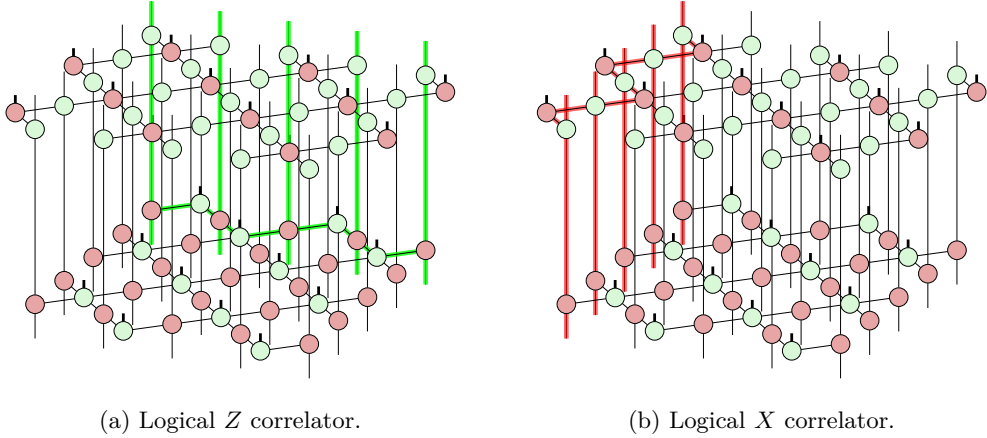


Figure 3: These are the logical  $Z$  and  $X$  correlators, linking the logical ( $Z$  and  $X$  respectively) operators of the surface code from the input (bottom legs) to the output (top legs).

the logical  $Z$  correlator is the green Pauli web (figure 3a), similarly, the logical  $X$  correlator is the red Pauli web (figure 3b). Note that the Pauli web colouring convention is the exact opposite of [9], following the colour map from [10].

### 2.3 Combined ZX-diagram

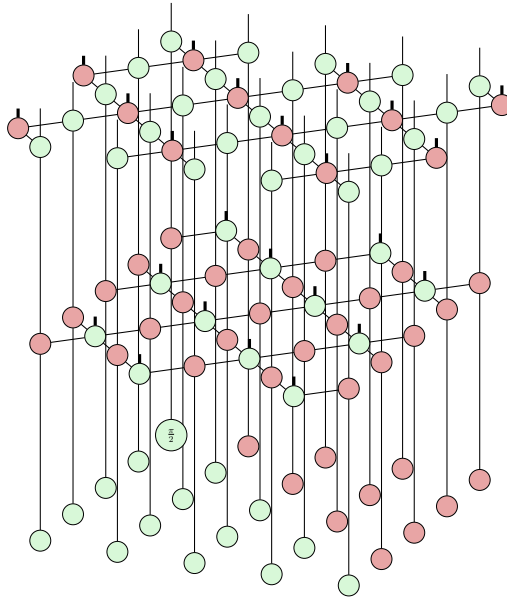


Figure 4: The surface code encoder circuit in figure 2 applied to the initial states (figure 1).

The combined ZX-diagram with initialisation and encoder circuit is shown in figure 4. Multiple rounds of parity measurement circuit should be stacked on top repeatedly in time to perform multi-round syndrome extractions. For simplicity, we shall ignore the 2 full rounds of parity measurements or the post-selection and distance growth specified in the Li/Lao-Crigger schemes [5, 6], as a single round of parity measurement captures the essence when a Pauli web is constructed in an error-free circuit.

### 3 Pauli web of the $|Y\rangle$ state injection scheme

Following the Pauli web notation of [10], we start with the  $\pi/2$  phase Z-spider in the ZX-diagram (figure 4) and choose definition 2.7 from [10]:

‘a spider with  $\pm\frac{\pi}{2}$  phase can have ... an odd number of legs highlighted in its own colour **and** all legs highlighted in the opposite colour’.

This leads to a multi-colour Pauli web decorated ZX-diagram as shown in figure 5a.

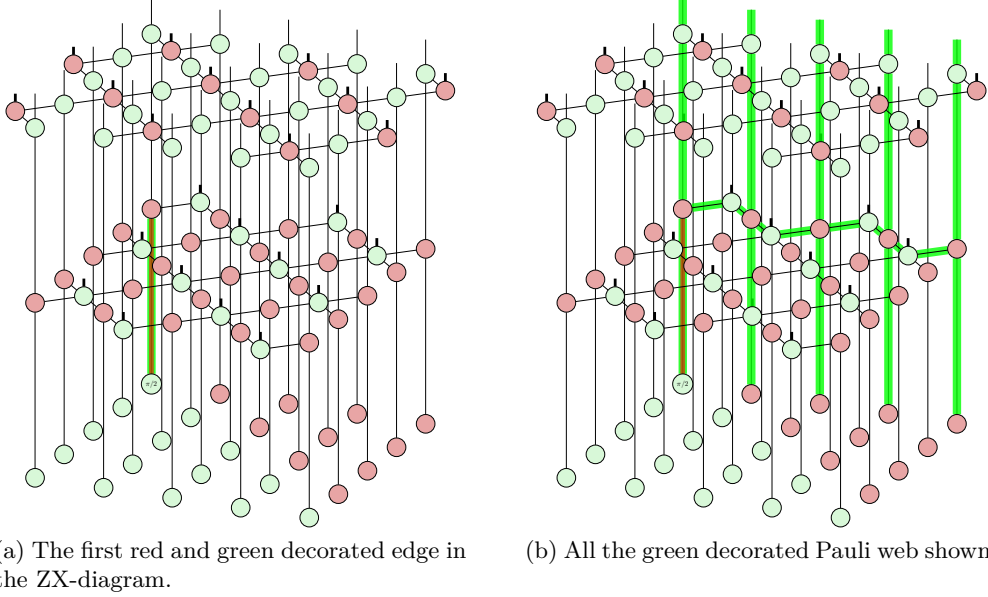


Figure 5

We shall then apply the other rules from definition 2.7 in [10]:

‘a spider with  $k\pi$  phase can have:

- an even number of legs highlighted in its own colour, and/or
- all or none of its legs highlighted in the opposite colour’

to find the green Pauli web first, by decorating all the phase-less spiders next, resulting in the ZX-diagram in figure 5b. Finally, we can work out the red decorated Pauli web, resulting in figure 6 using the same phase-less ( $k\pi = 0$ ) spider Pauli web rules. Figure 6 shows the logical correlator for a distance 5 surface code after 1 full round of error-free parity measurement. We can see that the Pauli web produced coincides with a logical  $Y$  correlator which is a combination of a logical  $X$  and logical  $Z$  correlator<sup>1</sup> as shown in figure 3.

### 4 Discussion

The “propagation” of the Pauli web to future rounds of parity measurement rounds and larger distances is straight forward. We suspect that similar approaches can be applied to

---

<sup>1</sup>Since  $iY = ZX$ .

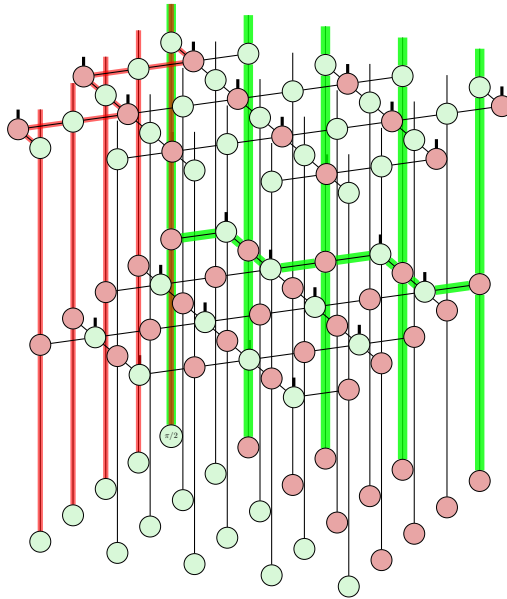


Figure 6: All the red and green decorated edge Pauli web shown. This recovers the logical  $Y$  correlators of the rotated surface code, which is the combination of the logical  $X$  and  $Z$  correlators.

replace the injected  $Z$ -spiders from  $\pi/2 \rightarrow \pi/4$  under appropriate Pauli web rule modifications [11] to diagrammatically visualise the  $|T\rangle$  state injection protocol [5, 6].

When we first read Li’s scheme [5] years ago, we were puzzled by the strange yet structured initialised qubit pattern. With ZX-calculus and Pauli web, we can see that if any of the states in the yellow highlighted rectangles (figure 7) are any different or of the opposite colour, the logical  $Y$  correlator Pauli web will not terminate properly. This will result in the incorrect logical  $Y$  correlator. Furthermore, the upper and lower triangular separated state initialisation supports the logical  $Y$  correlator and enables plaquette parity measurements needed for post-selecting clean injected states, as detailed in [5]. We shall provide a brief sketch on how to interpret the post-selection procedure at a superficial level in the next few subsections.

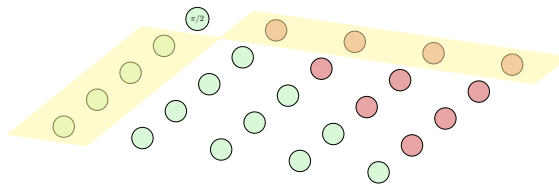


Figure 7: The initial states inside the yellow coloured rectangles must be green or red respectively in order to have the correct logical  $Y$  correlator [9].

#### 4.1 Parity measurements and syndrome extractions

In order to examine how to post-select in Li/Lao-Crigger’s schemes, let’s review how to perform error correction when a logical  $|0\rangle$  state is initialised (figure 8a). In the literature this is known as a ( $|\bar{0}\rangle$  initial state) memory experiment [4, 12]. For a distance  $d$  ( $= 5$  here) rotated surface code,  $n = d^2$  data qubits in the  $|0\rangle^{\otimes n}$  state will be initialised in the very first time slice. Following that, the encoder circuit from figure 2 is repeatedly applied. In figure 8a, we have applied 1.5 encoder circuit with the final half full-round

of parity measurements omitted for simplicity. Figure 8a shows one initial time  $Z$ -type *syndrome/parity check* to the  $|0\rangle$  memory experiment as a green decorated Pauli web [9]. Parity check is the product between consecutive rounds of parity measurements of the same type (i.e  $Z$  then  $Z$  or  $X$  then  $X$ ). If a Pauli  $X$  error occurred within the *parity check cube* in figure 8b, the product in parity measurements ( $1 \times -1 = -1$ ) will be non-trivial and hence we can potentially detect this error<sup>2</sup>.

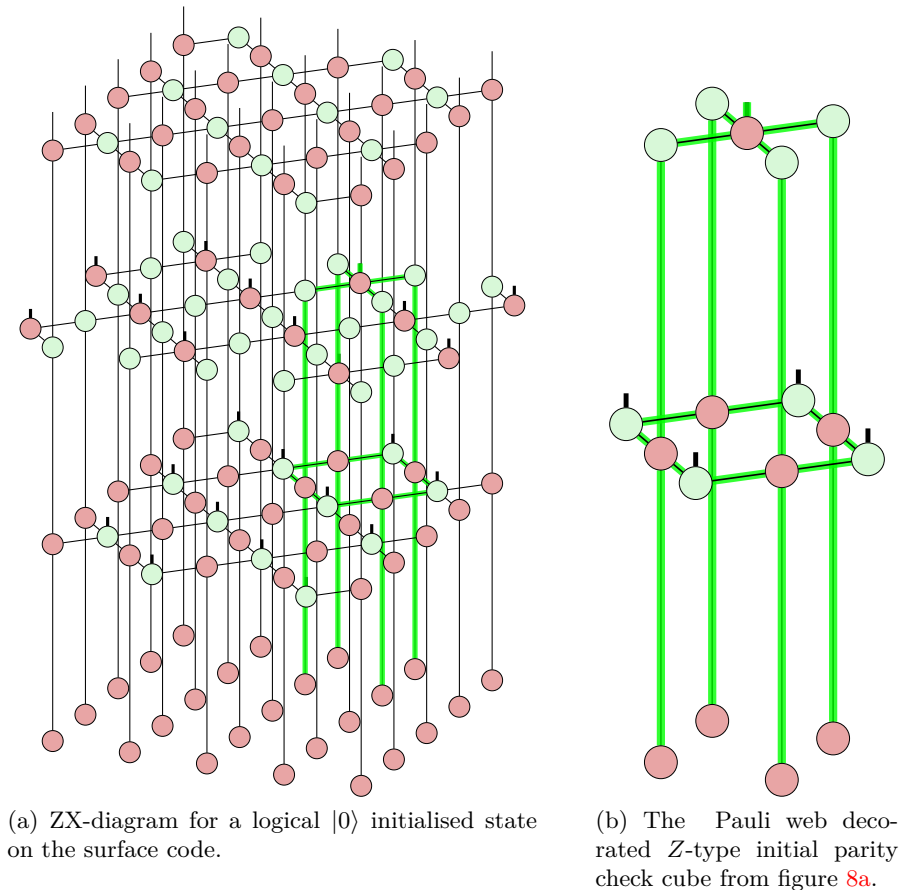


Figure 8

The curious reader will notice that the  $Z$ -type parity check cube in figure 8b is different<sup>3</sup> from the one shown in [9] as this parity check cube comes from the initial round of checks. Hence, the  $Z$ -type parity measurements will always be 1 if no errors occurred in the data qubits at the lowest time slice and  $-1$  if an error occurred on any data qubit above the lowest time slice<sup>4</sup>, shown as a  $\pi$   $X$ -spider in figure 9a. As a result, we do not need to perform a  $ZZZZ$  measurement on the very first time slice because we know  $ZZZZ = +1$  if no  $X$  errors occurred and  $-1$  otherwise. As it happens,  $|\bar{0}/\bar{1}\rangle, |\bar{+}/\bar{-}\rangle$  logical states can be fault-tolerantly initialised on the surface code. Starting from  $n = d^2$  data qubits in the  $|0/1\rangle^{\otimes n}$  (or  $|+/-\rangle^{\otimes n}$ ) separable state, measuring all the plaquette parities lead to a logical encoded  $X$  or  $Z$  eigenstate.

<sup>2</sup>Assuming appropriate decoding [4].

<sup>3</sup>Aside from the opposite Pauli web colouring convention.

<sup>4</sup>This is also known as initialisation error.

## 4.2 Data qubit error

Let's examine the consequence of a single data qubit  $X$  error after the first time slice on data qubit labelled **9** in cyan. Please note that all data qubit labelling will be written in cyan coloured font, **A** for example, and does not equate to a spider with phase  $A$ . The

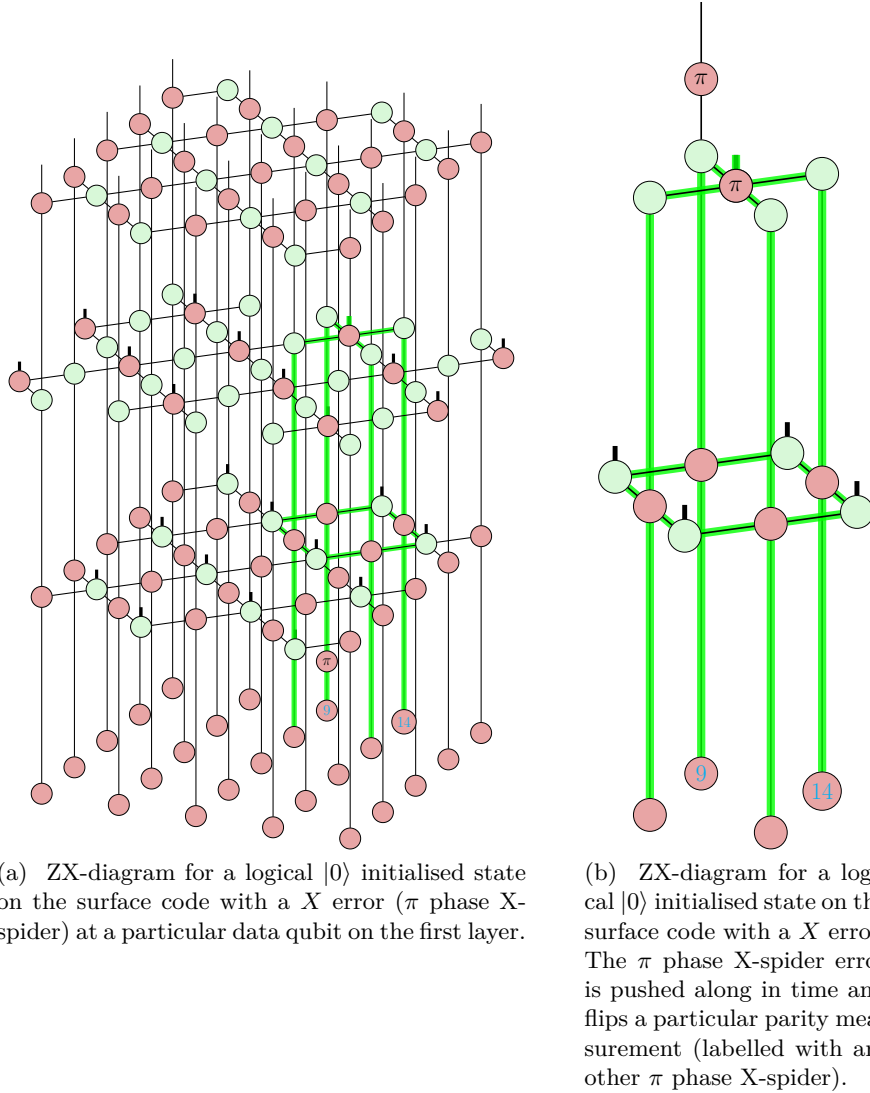


Figure 9

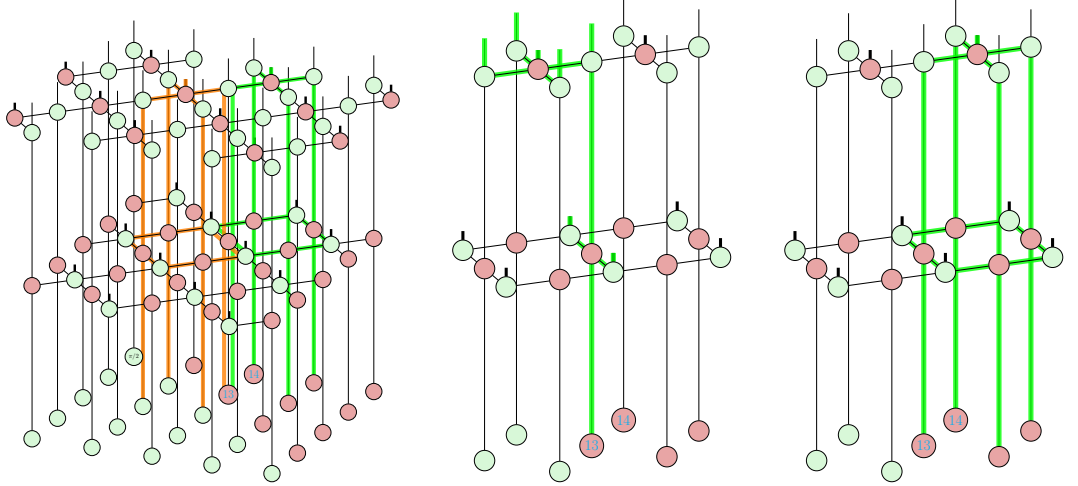
$\pi$  phase X-spider (Pauli  $X$  error) from figure 9a right after the first state initialisation time step on data qubit **9** can be pushed into future time layers with ZX-calculus. We can see that in figure 9a, the  $Z$  parity check at the third time slice picks up a  $X$  error ( $\pi$  phase X-spider) after pushing the  $\pi$  phase spider through. This means the parity check cube syndrome result will return  $-1$  in parity (or 1 in binary). On data qubit **9**, the Pauli frame is modified and the  $\pi$  phase X-spider persists in its world-line in time. If we perform minimum-weight perfect matching [4, 12, 13] to decode this syndrome, the syndrome<sup>5</sup> will be matched to the boundary of the decoding graph [12], hence we can infer that data qubit **9** or **14** (see figure 9b) had experienced a initialisation  $X$  error. The Pauli-frame will be

<sup>5</sup>Or a detector in PyMatching [12].

modified accordingly then.

### 4.3 $|Y\rangle$ state injection and post-selection

Let's examine two neighbouring parity check cubes in the  $|Y\rangle$  state injection protocol (figure 10).



(a) Two parity check cubes highlighted from the  $|Y\rangle$  state injection protocol associated with qubit 13. The orange Pauli web is also a 'green' Z-type Pauli web. It is coloured orange to make clear that it is an invalid Pauli web, as the orange Pauli web terminate on the initial states in an forbidden manner.

(b) The correct Pauli web associated with qubit 13 and the data qubits associated with the left orange (invalid) check cube.

(c) The right parity check cube from figure 10a.

Figure 10

We draw a left Z-type parity check cube (highlighted in orange instead of green for illustration and differentiation purposes) in figure 10a. This orange parity check cube is invalid as the initial green Z-spiders from the first time slices associated with it does not have the correct X-type, red Pauli web terminating on them. This invalid orange check cube has three  $|+\rangle$  states and one  $|0\rangle$  state in the first time slice dictated by the injection protocol. This implies that in the first time slice, the left orange check cube has  $ZZZZ = \pm 1$ , with either of the  $-1$  or  $+1$  value occurring with probability  $1/2$  when measured<sup>6</sup>. This means the measurement results associated with the left orange check cube cannot be reliably used to construct syndromes and infer errors when data qubit 14 (coloured cyan in figure 10) had experienced an initialisation error. Suppose the true initialisation  $X$  error is on data qubit 14. The right parity check cube will return a parity value of  $-1$ . However, the random parity measurement outcome in the left parity measurement could lead to the left parity check cube also returning a parity value of  $-1$ , hence we would have decoded and misidentified a  $X$  initial error on data qubit 13. This in turn leads to a mis-calculated

<sup>6</sup>Let's look at this in the stabiliser notation, if we were to measure  $Z_a Z_b Z_c Z_d$  in a system stabilised by  $\langle X_a, X_b, X_c, Z_d \rangle$ , these three stabiliser generators:  $X_a, X_b, X_c$  each anti-commutes with the measurement basis:  $Z_a Z_b Z_c Z_d$ . Hence, the resultant stabiliser generators post measurement is:  $\langle (-1)^m Z_a Z_b Z_c Z_d, X_a X_b, X_a X_c, Z_d \rangle$ , with the measured  $Z_a Z_b Z_c Z_d$  binary result,  $m \in \{0, 1\}$ , happening uniformly at random.



Pauli-frame concerning the logical  $Y$  correlator. One solution to overcome this is to then post-select  $+1$  parity measurement results in all the plaquettes labelled ‘ $+1$ ’ in figure 11, where we have a green  $X$ -type and red  $Z$ -type plaquettes rotated surface code [4]. This lowers the chances of misidentifying the Pauli-frame for the logical  $Y$  correlator, which leads to the high fidelity logical state injection, as shown in the Li [5] and Lao-Crigrer [6] schemes.

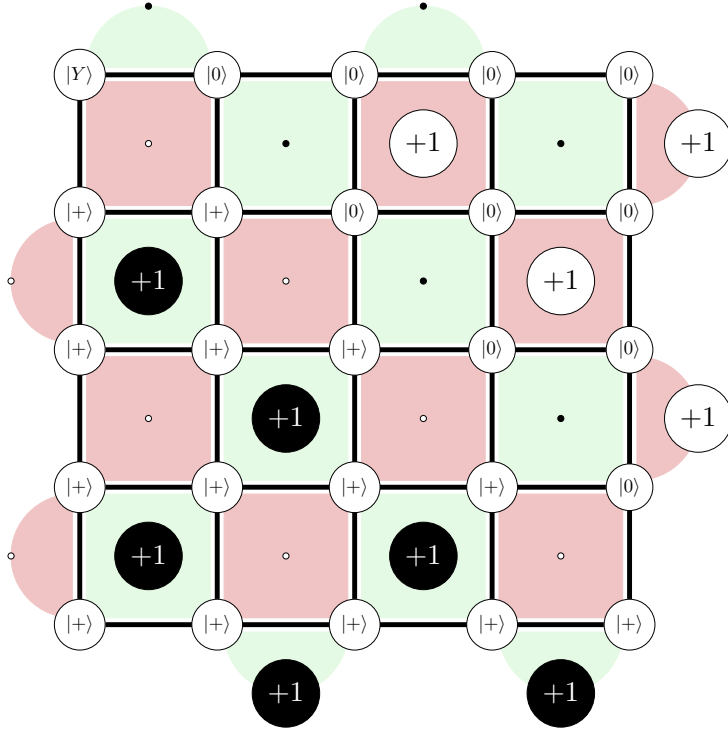


Figure 11: A distance  $d = 5$  rotated surface code with green  $X$ -type and red  $Z$ -type plaquettes. In the injection scheme, the  $+1$  labelled plaquettes are the parity measurements that one post-select on given a  $+1$  parity value (see detailed discussion in [5, 6]).

## 5 Acknowledgements

Kwok Ho Wan wishes to thank Zhenghao Zhong for a decade of friendship and also for inviting him to Oxford as a visitor whilst he was in between jobs. Zhenghao Zhong wants to thank Kwok Ho Wan for motivating him to write up these old ideas from their Imperial College London days. Zhenghao Zhong is currently supported by the ERC Consolidator Grant # 864828 “Algebraic Foundations of Supersymmetric Quantum Field Theory” (SCF-TAlg). Zhenghao Zhong acknowledges the TikZ code in figure 11 stems from Kwok Ho Wan’s personal lecture notes at Imperial College London and has explicit consent to use it.

## References

- [1] Daniel Gottesman. Stabilizer codes and quantum error correction, 1997. URL <https://arxiv.org/abs/quant-ph/9705052>.
- [2] Scott Aaronson and Daniel Gottesman. Improved simulation of stabilizer circuits.

- Physical Review A*, 70(5), November 2004. ISSN 1094-1622. DOI: [10.1103/physreva.70.052328](https://doi.org/10.1103/physreva.70.052328). URL <http://dx.doi.org/10.1103/PhysRevA.70.052328>.
- [3] Eric Dennis, Alexei Kitaev, Andrew Landahl, and John Preskill. Topological quantum memory. *Journal of Mathematical Physics*, 43(9):4452–4505, September 2002. ISSN 1089-7658. DOI: [10.1063/1.1499754](https://doi.org/10.1063/1.1499754). URL <http://dx.doi.org/10.1063/1.1499754>.
  - [4] Austin G. Fowler, Matteo Mariantoni, John M. Martinis, and Andrew N. Cleland. Surface codes: Towards practical large-scale quantum computation. *Physical Review A*, 86(3), September 2012. ISSN 1094-1622. DOI: [10.1103/physreva.86.032324](https://doi.org/10.1103/physreva.86.032324). URL <http://dx.doi.org/10.1103/PhysRevA.86.032324>.
  - [5] Ying Li. A magic state’s fidelity can be superior to the operations that created it. *New Journal of Physics*, 17(2):023037, February 2015. ISSN 1367-2630. DOI: [10.1088/1367-2630/17/2/023037](https://doi.org/10.1088/1367-2630/17/2/023037). URL <http://dx.doi.org/10.1088/1367-2630/17/2/023037>.
  - [6] Lingling Lao and Ben Criger. Magic state injection on the rotated surface code. In *Proceedings of the 19th ACM International Conference on Computing Frontiers, CF '22*, page 113–120, New York, NY, USA, 2022. Association for Computing Machinery. ISBN 9781450393386. DOI: [10.1145/3528416.3530237](https://doi.org/10.1145/3528416.3530237). URL <https://doi.org/10.1145/3528416.3530237>.
  - [7] Bob Coecke and Ross Duncan. Interacting quantum observables: categorical algebra and diagrammatics. *New Journal of Physics*, 13(4):043016, April 2011. ISSN 1367-2630. DOI: [10.1088/1367-2630/13/4/043016](https://doi.org/10.1088/1367-2630/13/4/043016). URL <http://dx.doi.org/10.1088/1367-2630/13/4/043016>.
  - [8] John van de Wetering. Zx-calculus for the working quantum computer scientist, 2020. URL <https://arxiv.org/abs/2012.13966>.
  - [9] Hector Bombin, Daniel Litinski, Naomi Nickerson, Fernando Pastawski, and Sam Roberts. Unifying flavors of fault tolerance with the zx calculus. *Quantum*, 8:1379, June 2024. ISSN 2521-327X. DOI: [10.22331/q-2024-06-18-1379](https://doi.org/10.22331/q-2024-06-18-1379). URL <http://dx.doi.org/10.22331/q-2024-06-18-1379>.
  - [10] Benjamin Rodatz, Boldizsár Poór, and Aleks Kissinger. Floquetifying stabiliser codes with distance-preserving rewrites, 2024. URL <https://arxiv.org/abs/2410.17240>.
  - [11] Aleks Kissinger and John van de Wetering. Simulating quantum circuits with zx-calculus reduced stabiliser decompositions. *Quantum Science and Technology*, 7(4):044001, July 2022. ISSN 2058-9565. DOI: [10.1088/2058-9565/ac5d20](https://doi.org/10.1088/2058-9565/ac5d20). URL <http://dx.doi.org/10.1088/2058-9565/ac5d20>.
  - [12] Oscar Higgott. Pymatching: A python package for decoding quantum codes with minimum-weight perfect matching, 2021. URL <https://arxiv.org/abs/2105.13082>.
  - [13] Oscar Higgott and Craig Gidney. Sparse blossom: correcting a million errors per core second with minimum-weight matching, 2025. URL <https://arxiv.org/abs/2303.15933>.